The Astrophysical Journal Letters, 752:L16 (6pp), 2012 June 10 doi:10.1088/2041-8205/752/1/L16

DISCOVERY OF SUPER-Li-RICH RED GIANTS IN DWARF SPHEROIDAL GALAXIES*

Evan N. Kirby[1,4], Xiaoting Fu[2], Puragra Guhathakurta[3], and Licai Deng[2]
[1] California Institute of Technology, 1200 E. California Blvd., MC 249-17, Pasadena, CA 91125, USA
[2] Key Laboratory of Optical Astronomy, National Astronomical Observatories, Chinese Academy of Sciences, Beijing 100012, China
[3] University of California Observatories/Lick Observatory, University of California, 1156 High St., Santa Cruz, CA 95064, USA
Received 2012 April 4; accepted 2012 May 3; published 2012 May 25

ABSTRACT

Stars destroy lithium (Li) in their normal evolution. The convective envelopes of evolved red giants reach temperatures of millions of kelvin, hot enough for the ^{7}Li$(p, \alpha)^4$He reaction to burn Li efficiently. Only about 1% of first-ascent red giants more luminous than the luminosity function bump in the red giant branch exhibit A(Li) > 1.5. Nonetheless, Li-rich red giants do exist. We present 15 Li-rich red giants—14 of which are new discoveries—among a sample of 2054 red giants in Milky Way dwarf satellite galaxies. Our sample more than doubles the number of low-mass, metal-poor ([Fe/H] $\lesssim -0.7$) Li-rich red giants, and it includes the most-metal-poor Li-enhanced star known ([Fe/H] $= -2.82$, $A(\mathrm{Li})_{\mathrm{NLTE}} = 3.15$). Because most of the stars have Li abundances larger than the universe's primordial value, the Li in these stars must have been created rather than saved from destruction. These Li-rich stars appear like other stars in the same galaxies in every measurable regard other than Li abundance. We consider the possibility that Li enrichment is a universal phase of evolution that affects all stars, and it seems rare only because it is brief.

Key words: galaxies: dwarf – Local Group – stars: abundances

Online-only material: color figures

1. INTRODUCTION

Before the first star was born, Li was the third-most-abundant element in the universe. In the intervening 14 Gyr between then and now, Li has been both created by spallation of carbon, nitrogen, and oxygen nuclei, and destroyed by astration in the interiors of stars. In most stars, destruction rates exceeded creation rates. Because stars produce rather than destroy most other elements, Li today is among the least abundant of the elements lighter than Zn.

In most metal-poor stars, the abundance of Li is a predictable function of surface temperature. Spectroscopy of large samples of stars in the Milky Way's halo (Spite & Spite 1982; Gratton et al. 2000) and in metal-poor globular clusters (Lind et al. 2009b; Mucciarelli et al. 2011) show that Li abundances in dwarf stars remain at the same value (A(Li) $= 2.3$)[5] until the first dredge-up on the subgiant branch. In this surface convection episode, material from deeper, hotter layers of the stars mixes with material at the stellar surface. The deeper layers contain no Li because Li burning is very efficient at $T \gtrsim 2.5 \times 10^6$ K, cool compared to hydrogen burning temperatures. As a result, the first dredge-up depletes the photospheric value of Li by a factor of 15–20 (Lind et al. 2009b).

Another dilution episode occurs at the luminosity function bump in the red giant branch (RGB). Extra mixing processes (e.g., Palmerini et al. 2011a) further introduce Li-depleted material to the stellar surface. The abundance of Li in red giants drops drastically as the star evolves beyond the RGB bump. After both dilution episodes, the number density of Li atoms drops to below 10 parts per trillion. Almost all first-ascent red giants with luminosities greater than the RGB bump have A(Li) < 1.5.

Some stars exhibit glaring exceptions to the standard picture of Li evolution. For example, excess Li often accompanies ^{13}C enhancement in CJ stars (Hatzidimitriou et al. 2003). These stars could have participated in "hot bottom burning" (a phrase coined by Scalo et al. 1975), wherein ^{7}Li can be synthesized in the star and observed at its surface. Specifically, the reaction ^{3}He$(\alpha, \gamma)^7$Be, part of the pp-II hydrogen burning chain, occurs at temperatures greater than 10^7 K. Li can be produced from Be by electron capture: ^{7}Be$(e^- \nu)^7$Li. However, the second reaction must occur at $T < 2.5 \times 10^6$ K, or else the Li will be destroyed by proton capture. The proposed Cameron–Fowler (1971) mechanism solves the temperature discrepancy by theorizing that ^{7}Be can be brought to the surface of the star, where it may capture an electron to create ^{7}Li. The stellar surface is cool enough to preserve Li. However, the ongoing convection guarantees that the surface Li atoms do not last long. They quickly return to destructive temperatures. Thus, the surface composition of Li is a balance between its creation by the Cameron–Fowler mechanism and its destruction by convection.

Hot bottom burning is effective at producing ^{7}Li in asymptotic giant branch (AGB) stars with masses of about 4–7 $M_\odot$ (Iben 1975; Sackmann & Boothroyd 1992). The convective envelopes of these stars reach layers where ^{7}Be is created. However, some less massive giants on both the RGB and AGB have been found to be Li-rich (e.g., Kraft et al. 1999; Palmerini et al. 2011a; Ruchti et al. 2011). The convective envelopes of these stars do not reach layers with ^{7}Be. Therefore, ^{7}Be should not be transported to the surfaces of these stars in the context of the standard model of stellar evolution. If the Cameron–Fowler mechanism is operating in these stars, then it requires "extra mixing" or "cool bottom processing" (Boothroyd et al. 1995; Sackmann & Boothroyd 1999) to connect the base of the

* The data presented herein were obtained at the W. M. Keck Observatory, which is operated as a scientific partnership among the California Institute of Technology, the University of California, and the National Aeronautics and Space Administration. The Observatory was made possible by the generous financial support of the W. M. Keck Foundation.
[4] Hubble Fellow.
[5] $A(\mathrm{Li}) = 12 + \log[n(\mathrm{Li})/n(\mathrm{H})]$ where n is the number density of atoms.

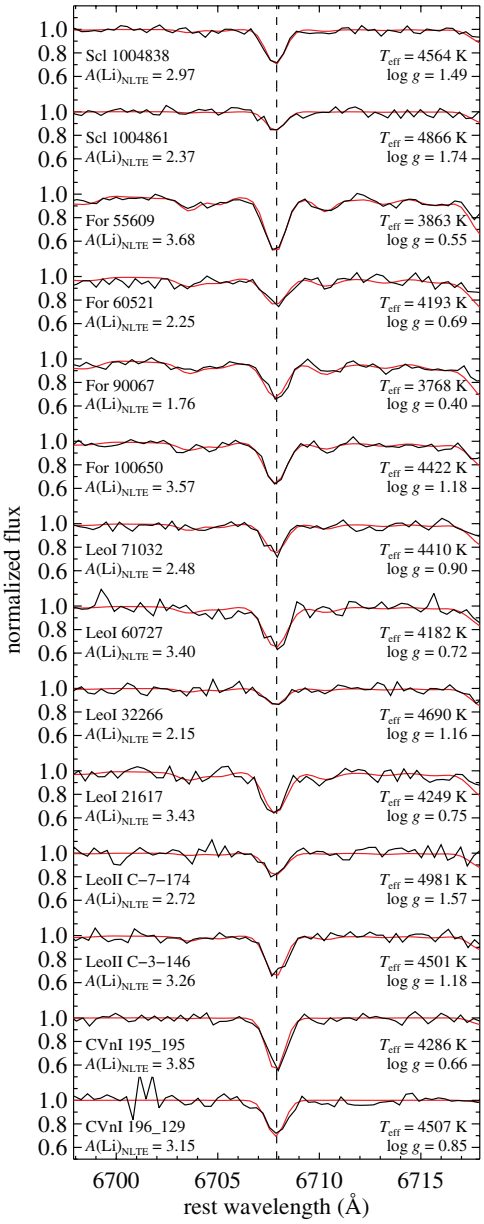

Figure 1. Small region of DEIMOS spectra centered on the Li I 6708 multiplet (dashed vertical line) for each of the 14 dSph giants with detectable Li. The observed spectra (black) have been normalized to have unit continuum. The red curves show the best-fitting synthetic spectra.

(A color version of this figure is available in the online journal.)

convective envelope to deeper regions of the star that contain Be. At one time, thermohaline convection was considered as a source of the extra mixing (Charbonnel & Zahn 2007), but the diffusion was later shown to be too slow to account for the photospheric compositions of red giants (Denissenkov & Merryfield 2011; Palmerini et al. 2011b). Alternative mixing processes include magnetic buoyancy (Nordhaus et al. 2008) and rotation (Charbonnel & Lagarde 2010).

Even though low-mass, Li-rich giants are rare, their existence challenges the standard theory of stellar evolution. They have spawned numerous modifications to the standard model. Different explanations depend on the evolutionary state of the star: the RGB bump (Charbonnel & Balachandran 2000), the AGB (Nollett et al. 2003), or even anywhere along the RGB (Sackmann & Boothroyd 1999). Furthermore, the composition of the star also influences the strength of extra mixing and therefore the surface abundance of Li (Sackmann & Boothroyd 1999).

Globular clusters and dwarf spheroidal galaxies (dSphs) are excellent places to search for Li-rich giants. First, they offer space densities high enough for efficient observations with multi-object spectrographs. Second, the stars are at a uniform distance, which eases the determination of evolutionary state and Li abundance.

2. LITHIUM MEASUREMENTS

Kirby et al. (2010) obtained spectra of nearly 3000 red giants in 8 dSphs with the DEIMOS medium-resolution, multi-object spectrograph (Faber et al. 2003) on the Keck II telescope. Of these data, 2812 spectra included the spectral region around the Li I resonance line at 6708 Å. The slit placement of the other stars caused their spectra to terminate redward of 6708 Å. We quantified the signal-to-noise ratios (S/Ns) of the spectra in the vicinity of the Li line by computing the inverse standard deviation of continuum-normalized pixels within 8 Å of the Li line but excluding the 4 Å immediately surrounding the line.

We searched for detections of the Li line in the 2054 spectra with S/N $>$ 10 pixel^{-1} that included the appropriate spectral range. We found 15 spectra with strong Li lines. The sample is random because the stars were not chosen for any property that could predict Li enhancement. One of these stars, star 461 in the Draco dSph, was already known to be Li-rich (Domínguez et al. 2004). The other stars belong to five dwarf galaxies: Sculptor, Fornax, Leo I, Leo II, and Canes Venatici I. This sample more than doubles the number of known Li-rich, metal-poor ([Fe/H] $\lesssim -0.7$) red giants.

Table 1 gives the identities of the 14 newly discovered, Li-rich stars. Because the stars reside in different galaxies, the photometry is not homogeneous. Table 1 gives the filter set in which each star was observed. Figure 1 shows the Li-rich stars' spectra around the Li line, and Table 2 gives the previously measured (Kirby et al. 2010) temperatures, surface gravities, microturbulent velocities, and metallicities for these stars.

We measured the equivalent widths (EWs) of the Li resonance lines by fitting Gaussians. In order to estimate the uncertainty on EW, we resampled the spectra 1000 times. In each realization, we perturbed the flux value of each pixel. The amount of perturbation was sampled from a Gaussian random distribution with a width equal to the measurement uncertainty of the pixel's flux. The EWs of the detected Li lines range from 175 to 694 mÅ. Table 2 gives the EWs. We measured the EWs only to illustrate that these lines are very strong and easily detected. We used spectral synthesis, not the EWs, to quantify the Li abundances.

The Li-rich stars' positions in color–magnitude diagrams (CMDs, Figure 2) are consistent with either the RGB or AGB. The colors and magnitudes of the two branches are hardly different for the old populations typical of dSphs. Whether the stars in our sample belong to the RGB or AGB, they belong to dwarf galaxies that are too old to host the 4–7 $M_{\odot}$ AGB stars that can produce Li in the standard model of stellar evolution (Sackmann & Boothroyd 1992). The colors of the Li-rich stars are also much redder than intermediate-mass AGB stars. Therefore, these low-mass stars are anomalous regardless of their evolutionary states.

We prepared each spectrum by normalizing to the continuum. We divided the observed spectrum by the best-fitting synthetic spectrum determined by Kirby et al. (2010). We fit a B-spline with a breakpoint spacing of 25 Å to the quotient spectrum,

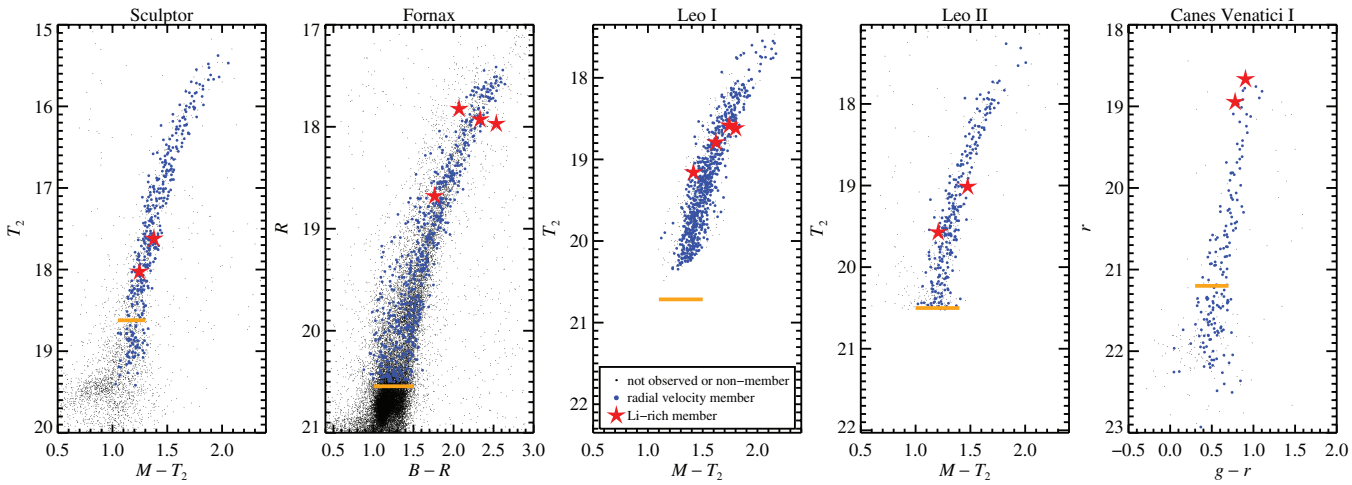

Figure 2. Color–magnitude diagrams for the dwarf galaxies in which Li-rich giants were detected. Blue points indicate radial velocity members. Red, five-pointed stars indicate the Li-rich stars, which are also radial velocity members. The orange horizontal lines indicate the approximate magnitudes of the RGB bumps. This magnitude was calculated with Ferraro et al.'s (1999) formula assuming the average age (Orban et al. 2008) and metallicity (Kirby et al. 2011) of the galaxy. The colors and magnitudes of the Li-rich stars indicate that they are low-mass giants more luminous than the RGB bump.

(A color version of this figure is available in the online journal.)

Table 1
Li-rich Red Giant Sample

Star Name	R.A. (J2000)	Decl. (J2000)	Filter 1	Mag 1	Filter 2	Mag 2	Approx. V	S/N at 6708 Å (pixel^{-1})
Scl 1004838	$00^h59^m34^s.1$	$-33°43'51''$	M	19.000	T_2	17.622	18.746	44
Scl 1004861	$00^h59^m34^s.2$	$-33°43'19''$	M	19.272	T_2	18.026	19.045	45
For 55609	$02^h39^m47^s.9$	$-34°27'47''$	B	20.260	R	17.928	18.887	38
For 60521	$02^h39^m52^s.0$	$-34°36'31''$	B	19.895	R	17.826	18.434	29
For 90067	$02^h40^m19^s.6$	$-34°33'42''$	B	20.506	R	17.971	18.969	50
For 100650	$02^h40^m31^s.3$	$-34°28'52''$	B	20.444	R	18.681	19.185	31
LeoI 71032	$10^h08^m17^s.6$	$+12°18'19''$	M	20.412	T_2	18.791	19.971	34
LeoI 60727	$10^h08^m18^s.0$	$+12°20'59''$	M	20.420	T_2	18.619	19.941	18
LeoI 32266	$10^h08^m30^s.1$	$+12°17'01''$	M	20.575	T_2	19.160	20.174	28
LeoI 21617	$10^h08^m37^s.3$	$+12°20'12''$	M	20.326	T_2	18.584	19.856	21
LeoII C-7-174	$11^h13^m19^s.0$	$+22°06'45''$	M	20.779	T_2	19.573	20.477	18
LeoII C-3-146	$11^h13^m36^s.2$	$+22°08'51''$	M	20.489	T_2	19.014	20.134	41
CVnI 195_195	$13^h28^m27^s.6$	$+33°36'43''$	g	19.571	r	18.667	19.044	37
CVnI 196_129	$13^h28^m44^s.3$	$+33°34'12''$	g	19.726	r	18.947	19.251	26

References. Identifications and photometry are from Westfall et al. (2006) for Sculptor, Stetson et al. (1998) for Fornax, Sohn et al. (2007) for Leo I and Leo II, and the Sloan Digital Sky Survey (Adelman-McCarthy et al. 2007) for Canes Venatici I.

Table 2
Stellar Parameters and Lithium Abundances

Star Name	$T_{\rm eff}$ (K)	$\log g$ (cm s^{-2})	ξ (km s^{-1})	[Fe/H]	EW(Li I 6708)	A(Li)$_{\rm LTE}$	A(Li)$_{\rm NLTE}$	$\sigma_{\rm noise}$	$\sigma_{T_{\rm eff}}$
Scl 1004838	4564	1.49	1.79	-1.59 ± 0.11	363 ± 19	3.32	2.97	0.12	0.24
Scl 1004861	4866	1.74	1.73	-1.70 ± 0.12	193 ± 29	2.46	2.37	0.15	0.15
For 55609	3863	0.55	2.01	-0.73 ± 0.11	694 ± 24	3.69	3.68	0.10	0.14
For 60521	4193	0.69	1.98	-0.86 ± 0.11	382 ± 35	2.11	2.25	0.13	0.20
For 90067	3768	0.40	2.05	-0.68 ± 0.11	503 ± 23	2.02	1.76	0.30	0.11
For 100650	4422	1.18	1.86	-0.95 ± 0.11	492 ± 28	3.74	3.57	0.14	0.22
LeoI 71032	4410	0.90	1.93	-1.29 ± 0.11	322 ± 27	2.50	2.48	0.15	0.23
LeoI 60727	4182	0.72	1.97	-1.42 ± 0.12	514 ± 47	3.49	3.40	0.39	0.19
LeoI 32266	4690	1.16	1.87	-1.35 ± 0.12	175 ± 30	2.07	2.15	0.13	0.17
LeoI 21617	4249	0.75	1.97	-1.10 ± 0.11	546 ± 52	3.53	3.43	0.37	0.19
LeoII C-7-174	4981	1.57	1.77	-1.24 ± 0.12	225 ± 42	2.92	2.72	0.15	0.16
LeoII C-3-146	4501	1.18	1.86	-1.40 ± 0.11	449 ± 30	3.52	3.26	0.16	0.33
CVnI 195_195	4286	0.66	1.99	-2.61 ± 0.12	527 ± 17	3.98	3.85	0.20	0.28
CVnI 196_129	4507	0.85	1.94	-2.82 ± 0.13	380 ± 36	3.64	3.15	0.23	0.27

excluding the region between 6705.9 Å and 6709.9 Å. This exclusion made the continuum determination insensitive to the strength of the Li resonance line. We divided the observed spectrum by the spline.

We synthesized the spectral region around the Li resonance line with the spectral synthesis code MOOG (Sneden 1973) coupled with ATLAS9 model atmospheres (Kurucz 1993; Kirby 2011) in local thermodynamic equilibrium (LTE). We calculated the surface gravity of each star based on its position in the CMD and interpolation in model isochrones (Demarque et al. 2004). The temperatures were based on a combination of photometry and spectroscopy (Kirby et al. 2010). The spectra were synthesized with the multiplet of ^{7}Li lines (Hobbs et al. 1999). We assumed that all of the Li was in the ^{7}Li isotope, as is typical for metal-poor stars (Asplund et al. 2006). The full spectral range synthesized was 6697.9–6717.9 Å. Although Li is by far the strongest line in a 5 Å window around 6708 Å, we supplemented the line list with atomic (including Fe I 6707) and molecular (CN, C_2, and MgH) transitions from elements other than Li. We adopted the same line list as Kirby et al. (2008).

We calculated Li abundances and their uncertainties by minimizing χ^2 (Equation (1)) between the observed and synthetic spectra using Levenberg–Marquardt optimization:

$$\chi^2 = \sum_{\lambda=6705.9\,\text{Å}}^{6709.9\,\text{Å}} \frac{(f(\lambda) - s(\lambda))^2}{\sigma(\lambda)^2}. \quad (1)$$

In Equation (1), f represents the continuum-normalized observed spectrum, s represents the synthetic spectrum, and σ^2 represents the variance of the observed spectrum, propagated through flat fielding and continuum normalization. We repeatedly computed synthetic spectra with varying Li abundances until the χ^2 reached a minimum and changed by less than one part in 10^5 between iterations. Figure 1 shows the best-fitting synthetic spectra in red. We applied corrections for deviations from LTE using Lind et al.'s (2009a) grid. In some cases, we extrapolated beyond the boundaries of the grid ($\log g < 1$ and $T_{\rm eff} < 4000$ K). Table 2 lists the LTE and non-LTE (NLTE) Li abundances for the 14 newly discovered Li-rich giants.

We calculated two sources of error: $\sigma_{\rm noise}$ and $\sigma_{T_{\rm eff}}$. The random error on A(Li) from spectral noise, $\sigma_{\rm noise}$, is the amount by which A(Li) can change before χ^2 increases by one. There is also some systematic error from the uncertain effective temperature of the star, the continuum placement, and uncertainties in the transition probabilities. The uncertainty on $T_{\rm eff}$ dominates the systematic error. The approximate uncertainty on $T_{\rm eff}$ for these relatively cool giants is 100 K. We determined this systematic error by recalculating the best-fitting value of A(Li) from synthetic spectra with $T_{\rm eff}$ both 100 K above and 100 K below the nominal value of $T_{\rm eff}$ determined by Kirby et al. (2010). We then corrected A(Li) for NLTE effects. The average of these deviations of A(Li) from the value computed with the unperturbed temperature is $\sigma_{T_{\rm eff}}$. Table 2 gives both $\sigma_{\rm noise}$ and $\sigma_{T_{\rm eff}}$.

3. DISCUSSION

The Li abundances range from $A(\text{Li})_{\rm NLTE} = 1.76$ to 3.85. The universe's primordial value of Li is A(Li) = 2.72 (Coc et al. 2012). Eight of the stars in our sample have larger Li abundances. Therefore, these stars have not merely refrained from participating in Li destruction. The Li in these stars must have been created since the Big Bang. Our discovery reasserts that the phenomenon of extreme Li enrichment in giants is not limited to the Milky Way. Furthermore, the phenomenon extends to very metal-poor stars. The two Li-rich stars in Canes Venatici I have [Fe/H] < -2.6.

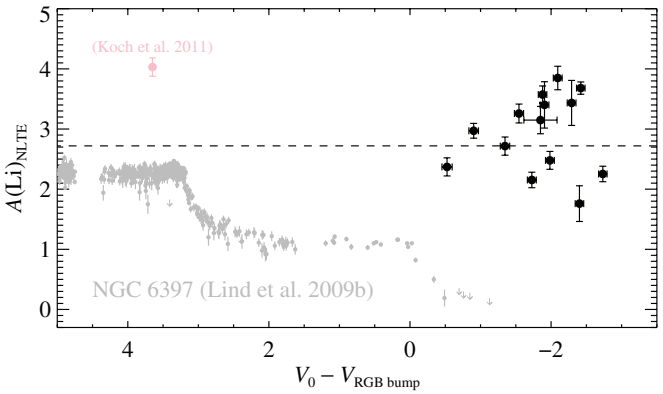

Figure 3. Li abundances as a function of the dSph stars' differences in V magnitude from the predicted magnitude of the RGB bump, calculated with Ferraro et al.'s (1999) formula, assuming the average age (Orban et al. 2008) of the dSph and the measured metallicity of the star (Kirby et al. 2010). The errors on A(Li) are given by $(\sigma^2_{\rm noise} + \sigma^2_{T_{\rm eff}})^{1/2}$. Also shown are Li abundances in the globular cluster NGC 6397 (gray points and upper limits; Lind et al. 2009b). The dSph giants in our sample are much more Li-enhanced than typical red giants, and many are more Li-rich than the universe's primordial Li abundance (Coc et al. 2012), indicated by the dashed line. NGC 6397 also contains an unusually Li-rich turn-off star (pink point; Koch et al. 2011).

(A color version of this figure is available in the online journal.)

Figure 3 shows A(Li) as a function of the evolutionary state of the star, expressed as a difference in magnitude from the RGB bump in the dSph. The RGB bump magnitude is calculated individually for each star from Ferraro et al.'s (1999) formula, assuming the mean age of the dSph (Orban et al. 2008) and the measured metallicity of the star (Kirby et al. 2010). For comparison, Figure 3 also includes Li abundances in the metal-poor globular cluster NGC 6397 from the main sequence through RGB bump (Lind et al. 2009b). Incidentally, NGC 6397 contains a Li-rich turn-off star, which is even harder to explain than Li-rich giants (Koch et al. 2011).

Like most other metal-poor, Li-rich giants (Ruchti et al. 2011), all of the stars in our sample are more luminous than the RGB bump. However, our sample is biased toward high luminosities. Of the stars we searched, 1764 out of 2054 (86%) are more luminous than the RGB bump, and the Li line at fixed abundance becomes weaker for decreasing luminosities (higher temperatures). Although our sample does not offer strong statistical evidence for the Li-rich phenomenon to occur exclusively above the RGB bump in metal-poor stars, all of the known, metal-poor, Li-rich giants are consistent with that hypothesis. Almost all of our sample's stars that are less luminous than the bump reside in galaxies without detections of Li-rich stars.

The fraction of strong Li detection in our sample of stars with S/N > 10 pixel^{-1} above the RGB bump is 15 of 1764 (0.85%). However, the detectability of Li depends on the stellar temperature, Li abundance, and spectral S/N. Our spectra with lower S/Ns could harbor anomalously large Li lines, but we possibly would have missed them in our visual search. Future work (X. Fu et al., in preparation) will make a more quantitative determination of the Li-rich fraction of red giants in our sample.

The existence of Li-rich red giants and their abundances do not correlate with any measurable parameter. Although Charbonnel & Balachandran (2000) found that Li-rich giants seem to cluster in the CMD, including at the RGB bump, our sample shows no such clustering. Lebzelter et al. (2012) found a similar result in the Milky Way bulge. Our sample and Lebzelter et al.'s sample have the advantage that the stars are in stellar systems with known distances. Therefore, the magnitude distance from the RGB bump does not need to be inferred from spectroscopically determined atmospheric parameters. In addition to positions in the CMD, our stars' temperatures, surface gravities, iron abundances, and [α/Fe] abundance ratios are not unusual in any regard with respect to Li-normal stars in the same dwarf galaxies. Although the resolution of our spectra is too low to measure rotation, at least 80% of metal-poor, Li-rich red giants in another survey (Ruchti et al. 2011) exhibit typical rotation velocities.

The typicality of metal-poor, Li-rich stars in all regards except Li abundance suggests that these stars are not unusual in terms of their intrinsic properties or external stimuli. Furthermore, the fraction of Li-rich, metal-poor giants in our sample shows that the frequency of the Li-rich phenomenon in dSphs—about 1%—is roughly the same as in the Milky Way disk, bulge, and halo (Brown et al. 1989; Ruchti et al. 2011; Lebzelter et al. 2012). The apparent randomness of giants that exhibit large Li abundances restricts extra mixing models. For example, the sudden increase in angular momentum caused by engulfment of a planet could induce extra mixing (Denissenkov & Weiss 2000). However, the occurrence of planets in the solar neighborhood is far more likely around metal-rich stars (Fischer & Valenti 2005). Assuming that stars in dSphs also obey a correlation between metallicity and the occurrence of hot Jupiters and that the occurrence relation extends to very low metallicities ($-3 <$ [Fe/H] < -0.5), the stars in our sample are extremely unlikely to host hot Jupiters. In fact, we could find no model in the literature that adequately explains the available observations for Li-rich, low-mass, metal-poor giants (Li enhancements as high as $A(\mathrm{Li}) = 3.9$ even near the tip of the RGB, no concentration in the CMD, weak correlation with rotation).

Because Li-rich, metal-poor giants are otherwise ordinary, we suggest that Li enhancement does not arise only in special cases. Instead, we echo a previous suggestion (de La Reza et al. 1996) that extra mixing and its associated Li enhancement could be a brief, universal phase of stellar evolution. The lifetime of a 10 Gyr old red giant is 420 Myr, 35 Myr of which is spent above the RGB bump (Dotter et al. 2008). The rate of Li depletion with increasing luminosity in NGC 6397 (Lind et al. 2009b) is roughly $\Delta A(\mathrm{Li})/\Delta M_V = 1.5$. Just above the RGB bump, red giants brighten by one magnitude in 19 Myr (Dotter et al. 2008). From these derivatives, we infer that the *e*-folding time for Li in the atmosphere of a normal, metal-poor red giant near the RGB bump is about 5 Myr, or 15% of the lifetime of the red giant above the RGB bump. However, the convection zone is deeper closer to the RGB tip than at the RGB bump, so the Li destruction rate must accelerate. Furthermore, the destruction rate could be even faster in the presence of extra mixing, which brings photospheric material to even hotter temperatures. The accelerated Li destruction could conspire to reduce the observable lifetime of an instantaneously Li-enhanced star to just 1% of the lifetime above the RGB bump. In this scenario, about 1% of all red giants above the bump would appear Li-rich. Palacios et al. (2001) postulated that this process happens in a Li flash that also serves to temporarily increase the luminosity of the red giant, which could explain why Li-rich giants are observed at all luminosities between the bump and the tip of the RGB. However, neither Denissenkov & Herwig (2004) nor Palacios et al. (2006) could achieve high enough mixing rates in their models to trigger a Li flash. Nonetheless, the idea that Li enhancement is a brief, universal phase of stellar evolution remains attractive in order to explain the lack of correlation with almost any other measurable parameter.

We thank the editor and the anonymous referee for a timely and helpful report. Support for this work was provided by NASA through Hubble Fellowship grant 51256.01 awarded to E.N.K. by the Space Telescope Science Institute, which is operated by the Association of Universities for Research in Astronomy, Inc., for NASA, under contract NAS 5-26555. X.T.F. and P.G. acknowledge support by NSF grant AST 09-37525. X.T.F. and L.D. thank NSFC for support by grants Nos. 10973015 and 11061120454. P.G. acknowledges NSF grant AST-1010039. The authors wish to recognize and acknowledge the very significant cultural role and reverence that the summit of Mauna Kea has always had within the indigenous Hawaiian community. We are most fortunate to have the opportunity to conduct observations from this mountain.

Facility: Keck:II (DEIMOS)

REFERENCES

Adelman-McCarthy, J. K., Agüeros, M. A., Allam, S. S., et al. 2007, ApJS, 172, 634
Asplund, M., Lambert, D. L., Nissen, P. E., Primas, F., & Smith, V. V. 2006, ApJ, 644, 229
Boothroyd, A. I., Sackmann, I.-J., & Wasserburg, G. J. 1995, ApJ, 442, L21
Brown, J. A., Sneden, C., Lambert, D. L., & Dutchover, E., Jr. 1989, ApJS, 71, 293
Cameron, A. G. W., & Fowler, W. A. 1971, ApJ, 164, 111
Charbonnel, C., & Balachandran, S. C. 2000, A&A, 359, 563
Charbonnel, C., & Lagarde, N. 2010, A&A, 522, A10
Charbonnel, C., & Zahn, J.-P. 2007, A&A, 467, L15
Coc, A., Goriely, S., Xu, Y., Saimpert, M., & Vangioni, E. 2012, ApJ, 744, 158
de La Reza, R., Drake, N. A., & da Silva, L. 1996, ApJ, 456, L115
Demarque, P., Woo, J.-H., Kim, Y.-C., & Yi, S. K. 2004, ApJS, 155, 667
Denissenkov, P. A., & Herwig, F. 2004, ApJ, 612, 1081
Denissenkov, P. A., & Merryfield, W. J. 2011, ApJ, 727, L8
Denissenkov, P. A., & Weiss, A. 2000, A&A, 358, L49
Domínguez, I., Abia, C., Straniero, O., Cristallo, S., & Pavlenko, Y. V. 2004, A&A, 422, 1045
Dotter, A., Chaboyer, B., Jevremović, D., et al. 2008, ApJS, 178, 89
Faber, S. M., Phillips, A. C., Kibrick, R. I., et al. 2003, Proc. SPIE, 4841, 1657
Ferraro, F. R., Messineo, M., Fusi Pecci, F., et al. 1999, AJ, 118, 1738
Fischer, D. A., & Valenti, J. 2005, ApJ, 622, 1102
Gratton, R. G., Sneden, C., Carretta, E., & Bragaglia, A. 2000, A&A, 354, 169
Hatzidimitriou, D., Morgan, D. H., Cannon, R. D., & Croke, B. F. W. 2003, MNRAS, 341, 1290
Hobbs, L. M., Thorburn, J. A., & Rebull, L. M. 1999, ApJ, 523, 797
Iben, I., Jr. 1975, ApJ, 196, 525
Kirby, E. N. 2011, PASP, 123, 531
Kirby, E. N., Guhathakurta, P., Simon, J. D., et al. 2010, ApJS, 191, 352
Kirby, E. N., Guhathakurta, P., & Sneden, C. 2008, ApJ, 682, 1217
Kirby, E. N., Lanfranchi, G. A., Simon, J. D., Cohen, J. G., & Guhathakurta, P. 2011, ApJ, 727, 78
Koch, A., Lind, K., & Rich, R. M. 2011, ApJ, 738, L29
Kraft, R. P., Peterson, R. C., Guhathakurta, P., et al. 1999, ApJ, 518, L53
Kurucz, R. 1993, in ATLAS9 Stellar Atmosphere Programs and 2 km/s grid, Kurucz CD-ROM No. 13, (Cambridge, MA: Smithsonian Astrophysical Observatory), 13
Lebzelter, T., Uttenthaler, S., Busso, M., Schultheis, M., & Aringer, B. 2012, A&A, 538, A36
Lind, K., Asplund, M., & Barklem, P. S. 2009a, A&A, 503, 541
Lind, K., Primas, F., Charbonnel, C., Grundahl, F., & Asplund, M. 2009b, A&A, 503, 545

Mucciarelli, A., Salaris, M., Lovisi, L., et al. 2011, MNRAS, 412, 81
Nollett, K. M., Busso, M., & Wasserburg, G. J. 2003, ApJ, 582, 1036
Nordhaus, J., Busso, M., Wasserburg, G. J., Blackman, E. G., & Palmerini, S. 2008, ApJ, 684, L29
Orban, C., Gnedin, O. Y., Weisz, D. R., et al. 2008, ApJ, 686, 1030
Palacios, A., Charbonnel, C., & Forestini, M. 2001, A&A, 375, L9
Palacios, A., Charbonnel, C., Talon, S., & Siess, L. 2006, A&A, 453, 261
Palmerini, S., Cristallo, S., Busso, M., et al. 2011a, ApJ, 741, 26
Palmerini, S., La Cognata, M., Cristallo, S., & Busso, M. 2011b, ApJ, 729, 3
Ruchti, G. R., Fulbright, J. P., Wyse, R. F. G., et al. 2011, ApJ, 743, 107
Sackmann, I.-J., & Boothroyd, A. I. 1992, ApJ, 392, L71
Sackmann, I.-J., & Boothroyd, A. I. 1999, ApJ, 510, 217
Scalo, J. M., Despain, K. H., & Ulrich, R. K. 1975, ApJ, 196, 805
Sneden, C. A. 1973, PhD thesis, Univ. Texas
Sohn, S. T., Majewski, S. R., Muñoz, R. R., et al. 2007, ApJ, 663, 960
Spite, F., & Spite, M. 1982, A&A, 115, 357
Stetson, P. B., Hesser, J. E., & Smecker-Hane, T. A. 1998, PASP, 110, 533
Westfall, K. B., Majewski, S. R., Ostheimer, J. C., et al. 2006, AJ, 131, 375